A Load Modulated Balanced Amplifier for Telecom Applications

Roberto Quaglia, *Member, IEEE*, and Steve Cripps, *Life Fellow, IEEE*

***Abstract*— This paper presents the design and characterization of a load modulated balanced amplifier for telecom base station applications adopting a novel mode of operation. The theory of operation is described explaining the main differences compared to Doherty amplifiers, in particular the RF bandwidth advantages and, on the other hand, the intrinsic nonlinear behavior. The specific design strategy that adopts prematching for back-off broadband matching is explained in detail. A prototype, based on 25-W GaN packaged devices, has been fabricated and measured with single tone CW and modulated signal stimulus. For CW conditions, on the 1.7–2.5-GHz band, the peak output power is between 63 and 78 W, with power added efficiency higher than 48%, 43%, and 39% at saturation, 6- and 8-dB output power back-off, respectively. With a modulated signal for Long Term Evolution the amplifier provides an average output power of around 10 W, with efficiency higher than 40%, and can be linearized by adopting a low complexity predistorter. If compared to previously published power amplifiers targeting similar power and bandwidth, the measurement shows very good performance, demonstrating the potential of this novel technique in the field of efficiency enhanced transmitters.**

***Index Terms*— Broadband matching networks, GaN-based FETs, wideband microwave amplifiers.**

I. Introduction

THE modern wireless communication standards rely on modulated signals characterized by high spectral efficiency in order to optimize the usage of the scarce spectrum resources. From the high-frequency transmitter perspective, this choice leads to stringent requirements in terms of linearity accompanied by a very high peak-to-average power ratio (PAPR) of the signals that force the power amplifier (PA) to operate at large back-off from saturation. While conventional PAs, as combined class-AB stages, show very low efficiency at back-off, there are widely adopted efficiency enhancement techniques that maintain high efficiency with high PAPR signals, i.e., bias modulation techniques as envelope tracking, and load modulation techniques as Doherty and Chireix [1].

A recent work [2] has introduced the load modulated balanced amplifier (LMBA), based on a balanced PA (BPA), where a control signal power (CSP) injected at the isolated port of the output 90° coupler modulates the load at each balanced device. A distinctive feature of the LMBA resides in the fact that, in principle, the CSP power is always fully recovered at the output of the LMBA, e.g., the CSP always positively contributes to the total output power, independently of the load modulation it is imposing. This situation is very different from the Doherty PA [3], [4], where the auxiliary output phase determines the load modulation on the main, but its power is fully recovered only when the phase is aligned with the main. This means that in a LMBA the load modulation and the CSP power recovery are independent, while in a Doherty the load modulation and the auxiliary power recovery are related. Another key property of the LMBA is RF bandwidth related; in fact, the load modulation is applicable for the whole frequency band of the 90° coupler that is normally larger than the bandwidth of a Doherty combiner [5]. The RF bandwidth enhancement has been at the center of the research on Doherty PAs for a long time, and several solutions have been found to achieve good bandwidth [5]–[12]. However, most of these techniques have proven to be quite complicated and often difficult to be applied beyond the specific case studied.

It is of great interest to explore a LMBA design tailored for telecom applications and assess pros and cons with respect to Doherty PAs. In this paper, a LMBA design strategy is proposed for the maximization of back-off efficiency. A prototype is realized targeting the 1.7–2.7-GHz frequency band, together with a maximum output power larger than 50 W, in order to provide a single PA solution for long-term evolution (LTE) small base stations at different frequencies. The CSP input is driven with a separate RF input for maximum flexibility in the testing of this new architecture. The use of dual-input in a load modulated architecture has led to a record 100% bandwidth in the PA of [10] (maximum power $\geq$ 20.5 W), where the output combiner is optimized to reach predefined targets when the two driving signals are assumed to be arbitrarily controllable in amplitude and phase. This added degree of freedom is paid for with a higher complexity, and the overall system must be evaluated case by case to decide if this approach is suitable in a specific application.

Previous literature has shown the use of a 90° coupler in a load modulated amplifier; the work in [11] uses a nonterminated branchline hybrid to realize the Doherty combiner reaching an RF bandwidth of 83% at maximum power larger than 10 W. However, the coupler in the LMBA is used in a fundamentally different way, as clearly explained in [2].

This paper proposes a new approach to efficiency enhanced PAs for telecom applications, and demonstrates through a

Manuscript received July 5, 2017; revised September 1, 2017; accepted October 5, 2017. Date of publication December 1, 2017; date of current version March 5, 2018. This work was supported by the European Union's Horizon 2020 Research and Innovation Programme under Marie Skłodowska-Curie Grant 654987. This paper is an expanded version from the IEEE MTT-S International Microwave Symposium Conference, Honolulu, HI, USA, June 4–9, 2017. *(Corresponding author: Roberto Quaglia.)*

The authors are with the Center for High Frequency Engineering, Cardiff University, Cardiff CF 24 3AA, U.K. (e-mail: quagliar@cardiff.ac.uk).

Color versions of one or more of the figures in this paper are available online at http://ieeexplore.ieee.org.

Digital Object Identifier 10.1109/TMTT.2017.2766066

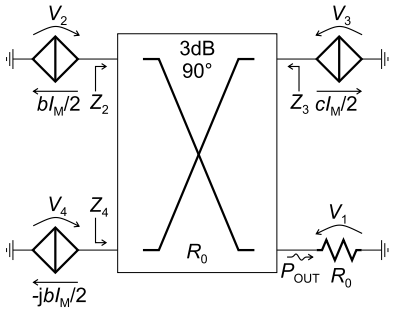

Fig. 1. LMBA: schematic for basic analysis.

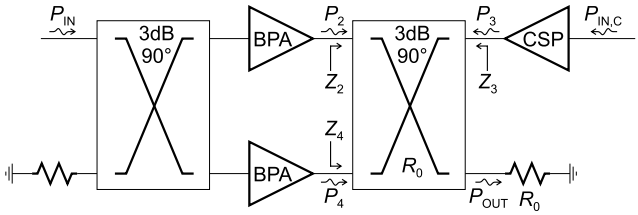

Fig. 2. LMBA for back-off efficiency enhancement.

prototype design that the LMBA has the potential to become a viable alternative to other techniques. The design follows easily reproducible steps, that can be adapted to different frequency bands, devices, and power levels.

The paper is organized as follows. Section II describes the theory of operation, the similarities and differences with Doherty PAs, and the proposed prematching method for the effective back-off efficiency maximization. The prototype design is discussed in detail in Section III, together with simulation results using nonlinear models. Section IV shows the characterization by means of CW and modulated signal measurements, and critically compares the results to other solutions from literature. Finally, Section V draws some conclusions.

II. Theory of Operation

A. Load Modulated Balanced Amplifier

The LMBA basic theory has been presented in [2]. Referring to Fig. 1, the impedance at each generator port can be written as

$$\begin{cases} Z_2 = Z_4 = R_0\left(1 + \dfrac{\sqrt{2}c}{b}\right) = Z_B \\ Z_3 = R_0 \end{cases} \tag{1}$$

where b and c are the drive levels of the balanced generators and the CSP generator, respectively, and R_0 is the coupler impedance. We assume b as a real value, while c is complex. The load presented to the balanced generators depends on the ratio between drive levels, (c/b), so it can be controlled in magnitude and phase by tuning the CSP generator amplitude and phase. Differing from other load modulated PAs, in [2] it is also shown that the CSP power always adds to the total output power P_{OUT} of the LMBA, independently of the phase of c

$$\begin{aligned} P_{\mathrm{OUT}} &= P_2 + P_4 + P_3 = 2P_B + P_3 \\ &= \frac{1}{8} R_0 I_M^2 \left| c + \sqrt{2} b \right|^2. \end{aligned} \tag{2}$$

The output power at each generator is P_2, P_3, and P_4, with $P_2 = P_4 = P_B$, while I_M corresponds to the maximum current deliverable by each of the balanced generators.

B. Back-Off Efficiency Enhancement

In this paper, the versatility of the LMBA concept is exploited to design a PA with good efficiency in back-off. Similar to a Doherty PA, the BPAs are ideally operating in class B, while the CSP is turned OFF ($c = 0$) in the input drive range $0 \le b \le \beta$, while it is turned ON for $\beta \le b \le 1$. This threshold behavior can be achieved by adopting a CSP device biased in class C and with proper power input power splitting or separate drive. The proposed topology is shown in Fig. 2: It can be noticed that the BPAs and the CSP PA are driven with independent frequency locked generators to allow for a greater freedom in the characterization. The harmonics are neglected in this analysis. At $b = \beta$, we assume that the BPA has achieved its maximum drain voltage $V_M = \beta R_0 \, I_M$, and as a consequence its maximum efficiency without clipping. This means that the native impedance R_0 must be set to $R_0 = R_{\mathrm{opt}}/\beta$, where R_{opt} is the optimum load for maximum power of the BPA.

To maintain high efficiency while further increasing the input drive, the voltage must be kept constant, leading to the identity

$$\beta I_M R_0 = \left(b + \sqrt{2}c\right) I_M R_0 \tag{3}$$

that imposes the following law for the CSP drive:

$$c = \begin{cases} 0, & 0 < b < \beta \\ \dfrac{1}{\sqrt{2}}(\beta - b), & \beta \le b \le 1. \end{cases} \tag{4}$$

The output power in the two drive regions can be evaluated

$$P_{\mathrm{OUT}} = \begin{cases} \dfrac{1}{4} b^2 R_0 I_M^2, & 0 < b < \beta \\ \dfrac{1}{16}(b+\beta)^2 R_0 I_M^2, & \beta < b < 1. \end{cases} \tag{5}$$

From this equation, the output back-off (OBO) can be calculated as the ratio of output power at $b = 1$ and $b = \beta$, and the result differs from the corresponding input back-off (IBO)

$$\begin{cases} \mathrm{IBO} & = 1/\beta^2 \\ \mathrm{OBO} & = (1+\beta)^2/(2\beta)^2 \end{cases} \tag{6}$$

meaning that the ideal proposed PA is intrinsically nonlinear, while a Doherty, at least in principle, is a linear PA. In the real operation of LMBA and Doherty Pas, other sources of weak and strong nonlinearity will also be present, as for example the nonconstant transconductance, the varactor effects, and the phase distortion induced by the load modulation [13]–[15]. Fig. 3 shows the CSP versus BPA function for different IBO values, while Figs. 4 and 5 show the load modulation and

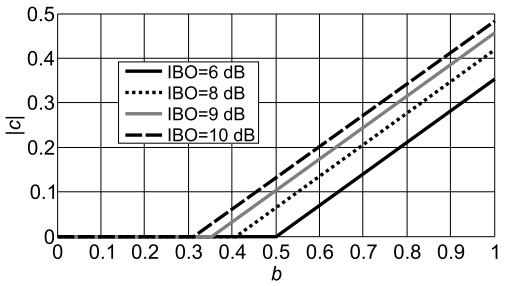

Fig. 3. CSP drive level c versus BPA drive b, for several IBO values.

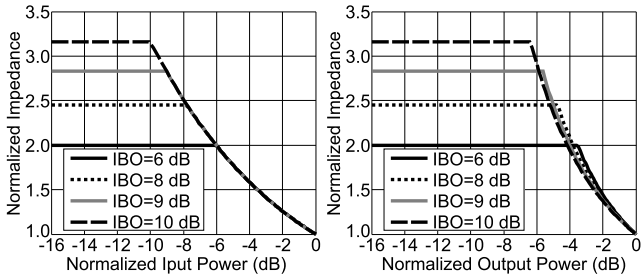

Fig. 4. Load modulation at BPA device. Impedance normalized to optimum load versus (left) balanced input power and (right) normalized output power, for different IBO values.

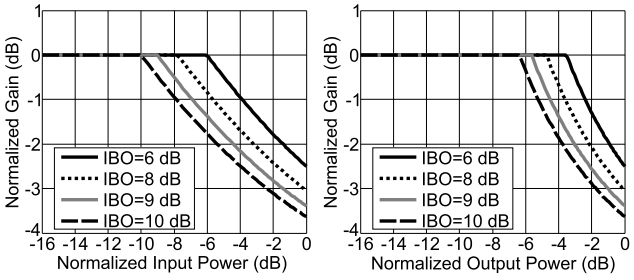

Fig. 5. Normalized gain versus (left) balanced input power and (right) normalized output power, for different IBO values.

normalized gain, respectively, at BPA device for some IBO values.

Recently, a LMBA prototype for telecom application has been proposed [16], however, this relied on a very different operation mode than the one presented in this paper. In particular, the early saturation of a CSP amplifier induces the load modulation into the BPA, meaning that the CSP operates also at low power drive.

C. Prematching

The proposed concept must be adapted to implementation with real microwave devices that operate on optimum impedances usually different from the feasible R_0 of a quadrature coupler. The optimum load is relatively low for high-power devices, and it is affected by the presence of the reactive and parasitic effects of the device. Although the LMBA could in principle compensate for this mismatch using active modulation alone, in order to maximize the added power provided by the CSP at saturation and minimize the impact of the CSP at back-off, a prematched solution has been preferred instead (see Fig. 6). In particular, on the

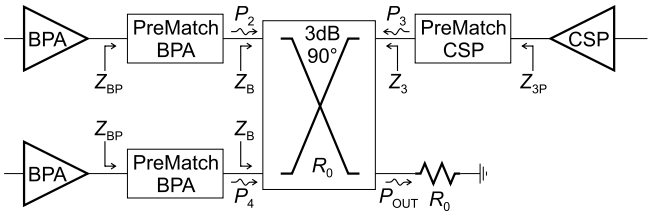

Fig. 6. LMBA with prematching: basic scheme.

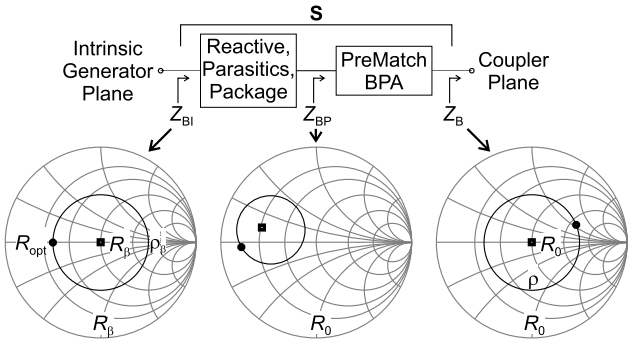

Fig. 7. Prematching: impedance transformation and reference planes.

BPA branches, the native impedance R_0 of the coupler is transformed to the extrinsic load corresponding to the intrinsic $R_{\rm opt}/\beta$ by a passive prematching network. Then, the active load modulation is used to impose the proper load condition during the progressive turning ON of the CSP.

It is important to understand the role of the prematching network in terms of load modulation. In particular, if compared to the ideal case without prematching, by imposing the same ratio of CSP to BPA power, is the same load modulation still achieved?

The equivalent network **S** comprising the cascade of device parasitics and prematching network (see Fig. 7) has the role of transforming $Z_B = R_0$ at the coupler plane to $Z_{\rm BI} = R_\beta = R_{\rm opt}/\beta$ at the intrinsic generator plane. As demonstrated in [17], assuming a lossless **S**, if a reflection coefficient ρ

$$\rho = \frac{Z_B - R_0}{Z_B + R_0} \tag{7}$$

is applied to port 2, it will be transformed to a reflection coefficient ρ_β

$$\rho_\beta = \frac{Z_{\rm BI} - R_\beta}{Z_{\rm BI} + R_\beta} \tag{8}$$

on port 1 with

$$|\rho_\beta| = |\rho|. \tag{9}$$

In [2], the reflection coefficient ρ at the balanced generator port was expressed in terms of the CSP-balanced device power ratio $\alpha = (P_3/P_B)$

$$|\rho|^2 = \frac{\alpha}{2+\alpha} \tag{10}$$

meaning that rotating the phase of the CSP drive, while maintaining its level, leads to ρ moving on a circle on the Smith Chart normalized to R_0. By applying (9), it is seen

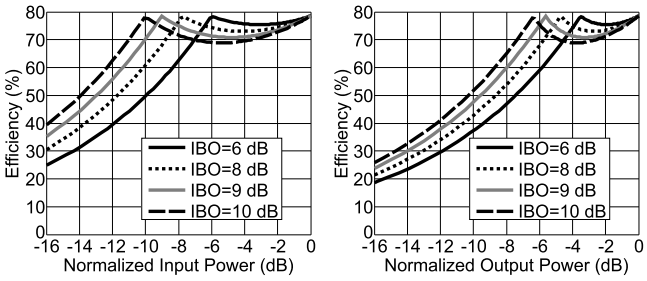

Fig. 8. Ideal drain efficiency versus (left) balanced input drive and (right) normalized output power, for several IBO levels.

also that ρ_β moves on a circle of the same radius. As a consequence, the amount of load modulation achieved at the coupler port is not degraded by the use of a prematching network, and is translated to the intrinsic device port except for a possible phase difference. Fig. 7 illustrates the principle of prematching by showing the translation of ρ from the coupler to the intrinsic plane. Different from a Doherty, in the proposed LMBA, the phase of the load modulation does not need to be adjusted by means of impedance inverters and offset lines, but can be tuned by changing the phase of the drive variable c by acting on the input of the CSP device. This difference can in principle mitigate some of the bandwidth limitations of the Doherty. The prematching network can be designed to achieve a rather large bandwidth, ensuring a good loading condition when the CSP is OFF. When the CSP operates, its phase can be imposed by a properly designed input splitter, or by separate CSP baseband control. In Fig. 7, it is also interesting to observe that, at the extrinsic plane of the device, the load modulation still leads to a circle, due to the conformal transformation imposed by the matching network. Regarding the CSP, the prematching network needs to transform $Z_3 = R_0$ to $R_{\text{opt,CSP}}$, i.e., the optimum load for maximum power/efficiency, at the intrinsic CSP device plane, in order to guarantee the maximum power delivery when the CSP is driven at full power. According to the theory, the CSP is a zero-current source when turned OFF, i.e., is an open circuit. However, with an ideal coupler, the actual phase of a reflective load does not impact on the load seen by the BPA devices, neither on the output power. This means, that at least ideally, the CSP turn-OFF condition is much more flexible than in the auxiliary of a Doherty PA, where the equivalent load seen from the common node should be designed as close as possible to an open circuit. This is often achieved through the insertion of an offset line, which limits the bandwidth [17], while in the LMBA this condition is in principle not needed. Considering ideal devices in class B bias, perfectly prematched according to the discussed strategy, the power consumption of the LMBA can be calculated as $P_{\text{DC}} = P_{\text{BPA,DC}} + P_{\text{CSP,DC}}$ of BPA and CSP can be calculated as follows:

$$\begin{cases} P_{\text{DC}} = \dfrac{R_0 I_M^2 \beta b}{\pi} + 0, & 0 < b < \beta \\ P_{\text{DC}} = \dfrac{R_0 I_M^2 \beta b}{\pi} + \dfrac{R_0 I_M^2 |\beta - b||\beta - 1|}{4\pi}, & \beta \le b \le 1. \end{cases} \tag{11}$$

Fig. 8 shows the ideal efficiency versus IBO and OBO.

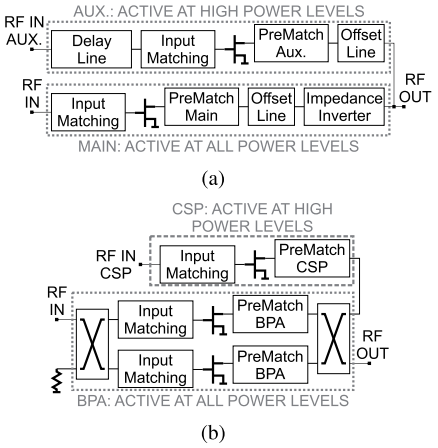

Fig. 9. Block diagram of (a) Doherty PA and (b) proposed LMBA.

D. Comparison With Doherty

Fig. 9 compares Doherty and LMBA schemes; for consistency, they are both considered with separate RF inputs. The main differences between the two architectures are as follows.

1) In Doherty, the main can be a single stage device while, in LMBA, the BPA is a balanced stage.
2) In Doherty, the two stages interact through current summation at a common node; in the LMBA, the output hybrid of the BPA is used to sum the CSP power.
3) In Doherty, to fully use the auxiliary power, its current must combine in phase with the main one at the common load; in the LMBA, CSP power is always recovered independently on its phase.
4) In Doherty, an impedance inverter is necessary to obtain the right load modulation; in the LMBA, the phase of the load modulation is tuned by the phase of the CSP drive.
5) In Doherty, the prematching network response can lead to the use of offset lines to maintain the right phase of the load modulation; in the LMBA, also with prematching, the phase of the load modulation can be controlled by the CSP input phase without the need of an offset line.

The last two observations are crucial in explaining the potential RF broadband capability of the LMBA. On the other hand, regarding instantaneous bandwidth, the LMBA might be more critical than a Doherty. In fact, the latter is naturally more symmetrical, meaning that the delay between the two branches is similar (identical in a first approximation); the modulated signal will be more likely to sum in phase at the common node not only a center frequency, but also on a broad bandwidth around it. For this reason, particular care must be taken when using a broadband signal with LMBA, and phase equalization algorithms should be considered at DSP level when splitting the baseband signals between the two modulators to generate the BPA and CSP signals. Fig. 10 shows the gain compression and efficiency versus OBO comparing Doherty and LMBA, assuming for simplicity all devices as ideal and with class B bias, and with break point at 6-dB OBO. Assuming that the CSP and auxiliary are driven to maintain constant drain voltage between break point and maximum power on main and BPA,

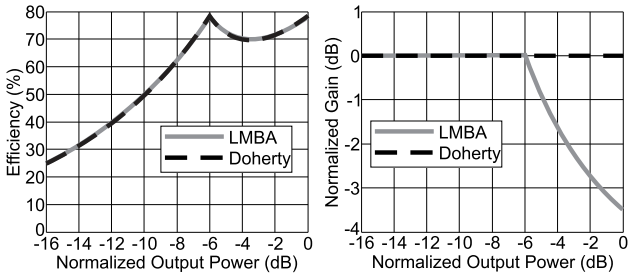

Fig. 10. (Left) Ideal drain efficiency and (right) normalized gain versus normalized output power, comparing Doherty and LMBA.

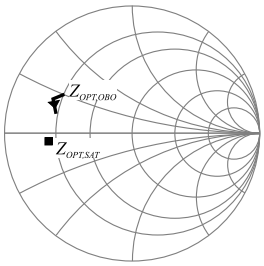

Fig. 11. Optimum loads for saturation and back-off in the 1.7–2.7-GHz band, referred to 50 Ω.

respectively, the efficiency curves result the same. The main difference is in the gain compression, clearly visible observing the compressive behavior of the LMBA in Fig. 10, while the Doherty is in first approximation linear. In fact, the break point at 6-dB OBO corresponds, in the ideal Doherty, to a break point at 6-dB IBO while, in the LMBA, the break point must be set at $\simeq$ 9.5-dB IBO.

III. Design

A. Active Devices

To test experimentally the proposed design strategy, a LMBA prototype has been designed targeting the 1.7–2.7-GHz frequency range and an output power higher than 50 W, both reasonable for small cell base stations for LTE.

The adopted active device for the BPAs is the CGH40025F from Wolfspeed Inc., a 28-V GaN on SiC HEMT in package, with 25-W nominal output power. The foundry provides an ADS nonlinear model, used in the initial phase of the design to identify the optimum loads across the design frequency band. In particular, the maximum power optimum load and the optimum load for efficiency at an IBO $\simeq$ 8 dB are shown in Fig. 11; the package pin reference plane is considered.

B. Hybrid Coupler

To mitigate the impedance transformation from R_0 to the optimum loads of Fig. 11, the coupler impedance can be reduced, offering advantages in terms of bandwidth, but most likely excluding the possibility of using off-the-shelf couplers that are normally matched on 50 Ω. In this design, an *ad hoc* microstrip branch-line coupler has been designed with reduced impedance. To achieve a target bandwidth of 1.7–2.7 GHz, the design approach of [18] has been followed, eventually obtaining a $R_0 = 25 - \Omega$ coupler with three sections.

The schematic and the electromagnetic-simulated, designed on a 508-μm substrate with $\epsilon_r = 2.2$, are shown in Figs. 12 and 13, respectively.

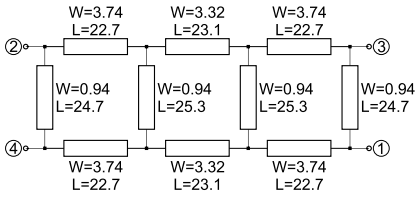

Fig. 12. Schematic of the branchline coupler. Length and width in mm.

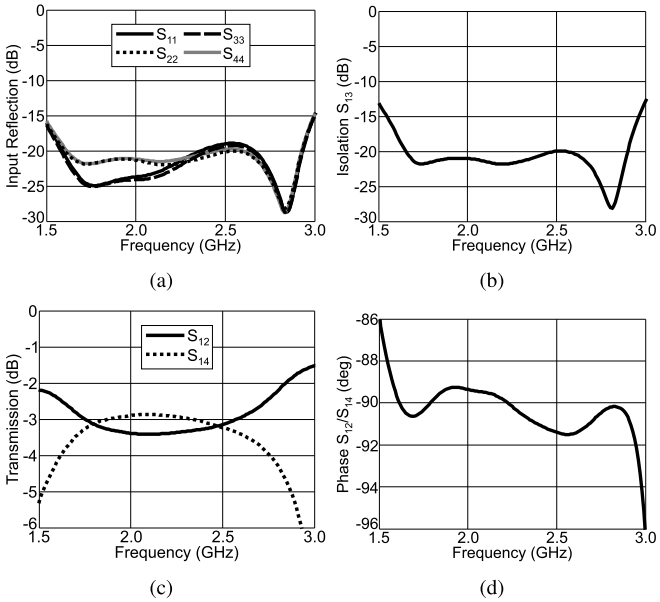

(a) (b) (c) (d)

Fig. 13. Electromagnetic scattering simulation results of the branchline coupler, with $R_0 = 25$ Ω.

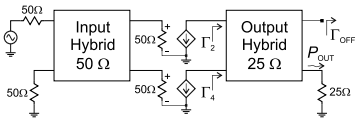

Fig. 14. Simulation setup for the assessment of real coupler effect.

Fig. 13 shows that the real coupler is characterized by amplitude/phase imbalance and finite isolation. To assess the impact of these imperfections, the schematic of Fig. 14 has been simulated, where ideal controlled current sources represent the BPA devices, while the CSP in OFF condition is represented by a unitary reflection coefficient Γ_{OFF} with arbitrary phase. A first simulation with ideal couplers is used to determine a normalization factor for the output power. Then, a simulation adopting the *S*-parameters of the real coupler is performed. Fig. 15 shows the normalized output power and the load seen by the BPA devices (Γ_2, Γ_4, referred to 25 Ω). The thick black lines represent the results obtained with $\Gamma_{OFF} = 1$, i.e., CSP as an open circuit, and highlight the impact of the real couplers, while the gray lines are obtained sweeping the phase of Γ_{OFF}, and show the effect of a non-open circuit CSP. First, it is interesting to notice that an open circuit is not always the optimum load condition. Moreover, the variation due to the phase sweep of the load is never too large, not even in a short circuit condition. This is in sharp contrast with a Doherty PA, where the auxiliary loading

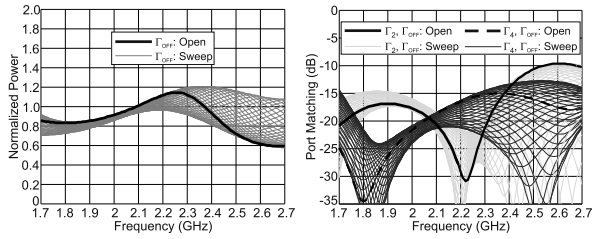

Fig. 15. Simulation results for the assessment of real coupler effect. (a) Normalized output power. (b) Γ_2, Γ_4. $\Gamma_{OFF} = 1$ (black thick line). Γ_{OFF} with swept phase (gray lines).

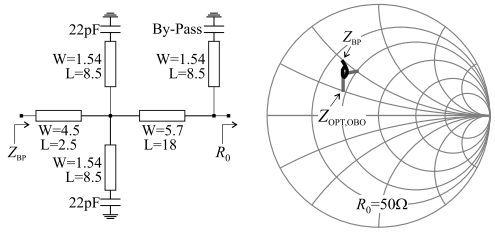

Fig. 16. Schematic of the BPA prematch, length and width in mm, and simulated impedance synthesized at the device pin level.

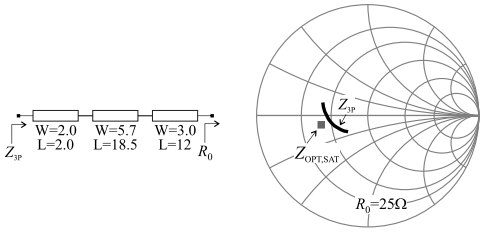

Fig. 17. Schematic of the CSP prematch, length and width in mm, and simulated impedance synthesized at the device pin level.

the common node with a low impedance would deteriorate dramatically the output power and the load at the main port. This is another intrinsic advantage of the LMBA with respect to a Doherty PA, and it can be enhanced by improving the hybrid coupler performance.

C. Prematching and CSP

The BPA prematching is designed to transform, over the design bandwidth, the coupler impedance $R_0 = 25\ \Omega$ to the optimum back-off terminations. Fig. 16 shows the microstrip schematic of the BPA prematch and the simulated synthesized load in the band 1.7–2.7 GHz. A preliminary simulation has been performed to ascertain the power needed at the CSP port, in order to identify a proper active device to implement the CSP PA. A CSP output power higher than 20 W is needed to cover the whole band; the same device of the BPA, the CGH40025F, has been selected. The CSP prematch needs to transform R_0 to the optimum at saturation for the device; the schematic and the simulated performance are shown in Fig. 17.

The use of a coupler with $R_0 = 25\ \Omega$ requires a global matching to 50Ω, which is obtained in our design using the circuit in Fig. 18, where the performance is also reported.

The input matching and broadband stabilization are provided by the network, identical for the three devices, shown

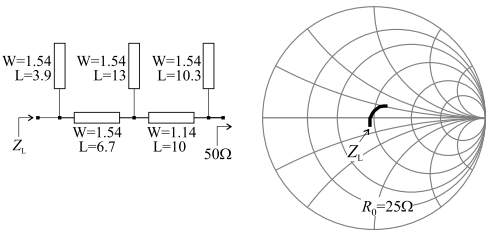

Fig. 18. Schematic of the output global matching, length and width in mm, and simulated matching results.

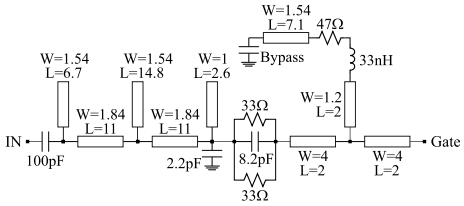

Fig. 19. Schematic of the input matching network, including broadband stabilization.

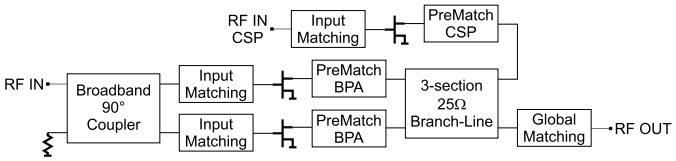

Fig. 20. Block diagram of the designed LMBA.

in Fig. 19. An off-the-shelf input coupler, the IPP-2004 from Innovative Power Products, is used at the input of the balanced amplifier, while the CSP input is independent, in order to test different options for its drive. The complete block diagram of the LMBA is shown in Fig. 20.

General design guidelines are as follows.

1) Identify frequency band and power requirements, and select proper active devices for the BPAs.
2) Locate R_{opt} and R_{opt}/β, or their corresponding extrinsic loads.
3) Select or design a 90° coupler covering the frequency band, possibly with R_0 close to R_{opt}/β to relax prematching constraints.
4) Design BPA prematching.
5) Identify CSP requirements and select CSP device.
6) Locate CSP optimum load and design CSP prematching.
7) Design output matching, input matching, and stabilization.

D. Simulation Results

The matching networks have been slightly tuned through large signal simulations, adopting the foundry nonlinear model, in order to achieve in the 1.7–2.7 GHz an output power higher than 75 W, and a back-off efficiency, at 6–8-dB OBO, as high as possible. The harmonics, especially the second, have been monitored to avoid detrimental conditions for power and efficiency. The efficiency being considered throughout this paper is the power added efficiency (PAE) that accounts for both RF input power

$$\mathrm{PAE} = 100 \times \frac{P_{\mathrm{OUT}} - P_{\mathrm{IN}} - P_{\mathrm{IN},C}}{P_{\mathrm{DC}}}. \tag{12}$$

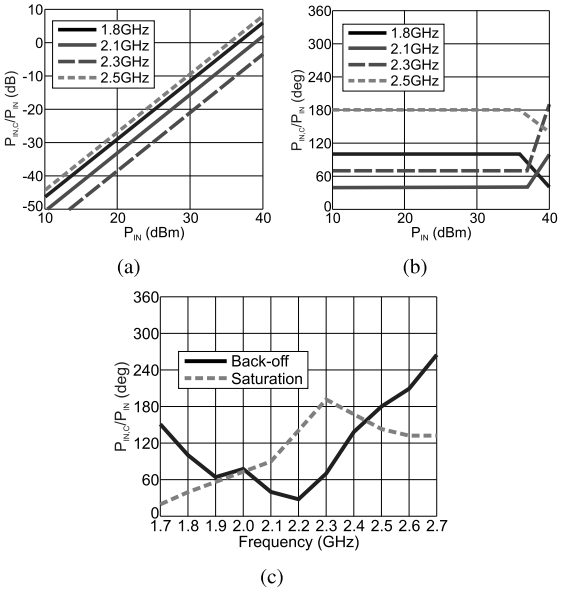

Fig. 21. Applied CSP input, ratio to BPA input. (a) Amplitude and (b) phase versus input power. (c) Phase versus frequency.

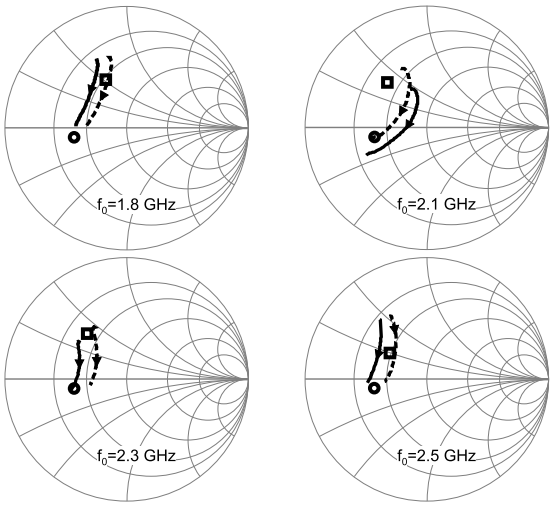

Fig. 22. Load modulation at BPA devices versus drive at selected frequencies, referred to $R_0 = 25\ \Omega$. Port 2 (Dotted line) and Port 4 (solid line). Optimum load at saturation (circle) and back-off (square).

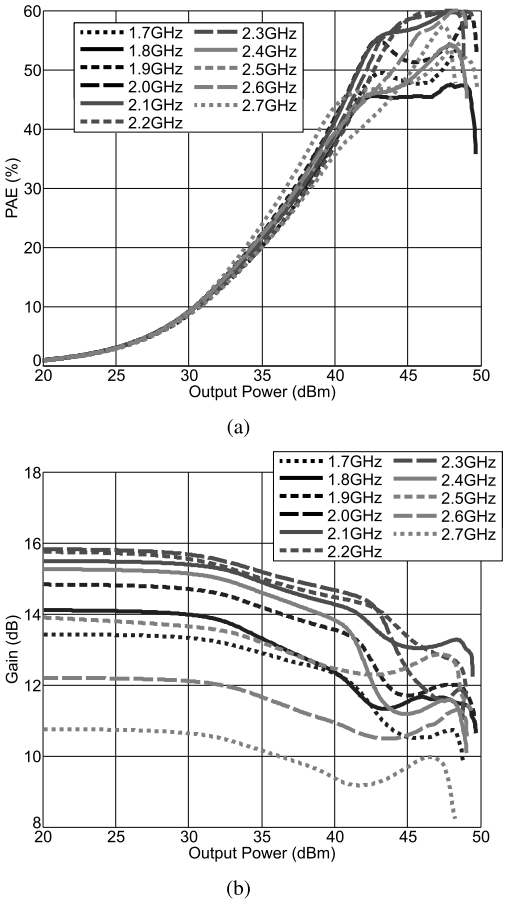

Fig. 23. Simulated CW power sweep in the range 1.7–2.7 GHz. (a) PAE versus output power. (b) Gain versus output power.

Given the flexibility in driving the CSP device, the amplitude and phase profiles of the CSP input can be adjusted to meet different specifications, for example, by creating a lookup table from extensive simulations with nested sweeps. However, these simulations can be very time consuming, and the resulting look-up tables difficult to implement in a real system with modulated signals. As a simplification, the amplitude relation between CSP and BPA has been described by a near quadratic form, or in dB, by a 1.8:1 relation, a value selected after some initial manual tuning of the CSP power level. Regarding the phase, a constant phase has been applied up to a specified drive, while a linear degree/dB slope is applied for higher power. The absolute power, phase difference, and the phase slope have been tuned at each frequency to achieve the maximum power level and the best back-off efficiency. As an example, Fig. 21 shows the applied amplitude/phase relation at some frequencies. The resulting load modulation at BPA devices, at some frequencies, is represented in Fig. 22. Fig. 23 shows the simulated efficiency versus output power for different frequencies, while Fig. 24 shows the simulated output power, saturated PAE, back-off PAE and gain versus CW frequency. It is important to notice that, compared to a standard Doherty, an LMBA requires three devices instead of two. However, this does not automatically implies a cost increase of 150%. The reason is that the CSP device power is recovered, and as a consequence three smaller devices can be used instead of two larger ones to achieve the same power, with a cost increase that must evaluated case by case.

IV. Characterization

A. Scattering

The LMBA has been fabricated and mounted on an aluminum carrier, using SMA coaxial launchers for accessing the RF ports (see Fig. 25 for a photograph of the hardware). Scattering measurements have been carried out for an initial assessment of performance and agreement with simulations. Fig. 26 shows the comparison of simulated and measured scattering (input matching and transmission) in two conditions. On the left column, the path from BPAs input to output is considered, with the BPAs biased at 28 V and 250 mA

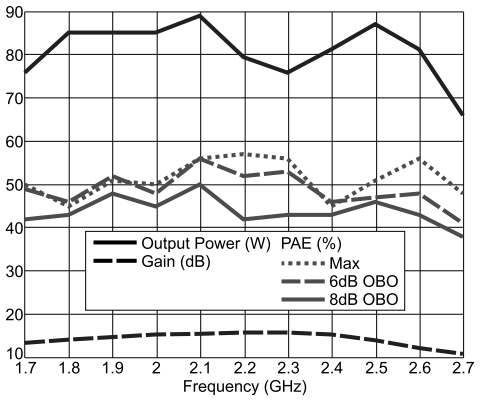

Fig. 24. CW simulation results versus center frequency.

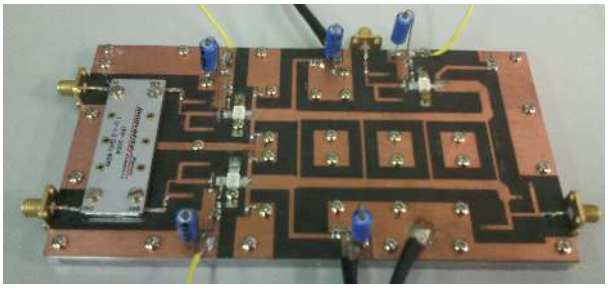

Fig. 25. Photograph of the fabricated LMBA.

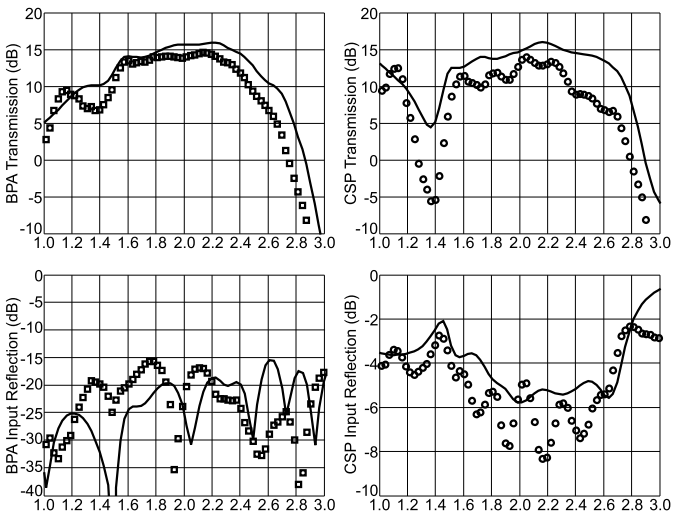

Fig. 26. Scattering parameters: measured (symbols) and simulated (lines). BPA with CSP OFF (left column). CSP with BPA OFF (right column).

per device, and the CSP in class C (28 V, gate voltage at −3.9 V). On the other hand, on the right column, the path from CSP input to output is represented, with the BPA devices in class C (28 V, gate voltage at −3.9 V), and the CSP at 28 V and 250 mA. In both cases, the agreement of the transmission parameter with simulations is rather good, with a band reduction at higher frequencies of around 200 MHz in measurements, reducing the useful bandwidth to 1.7–2.5 GHz. Matching results are very good for the BPAs, as expected from a balanced stage, and in good agreement with simulations in the CSP.

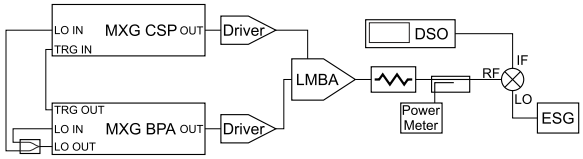

Fig. 27. Diagram of the measurement setup.

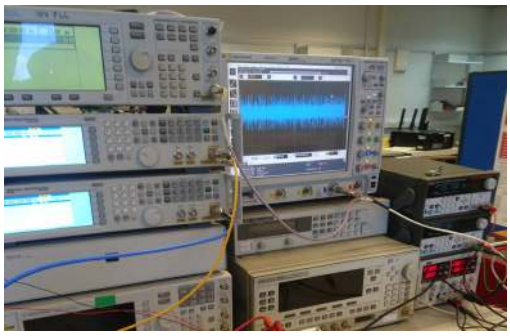

Fig. 28. Photograph of the measurement setup.

B. Measurement Setup

The independent control of BPA and CSP inputs permits a full investigation of the potential of the LMBA. In our measurements, the generation of the two independent modulated signals has been achieved by synchronizing two Keysight MXG N5182B generators, in order to obtain good baseband and carrier phase alignment of the channels. It has to be noticed that, in a real radio, a single clock, and a single local oscillator would be used to drive the signal processing and the modulators, hence the issue of synchronization is less critical than in our scenario. Figs. 27 and 28 show the block diagram and a photograph, respectively, of the characterization setup. Linear drivers are used to amplify the generated signals to a proper level for the DUT. The DUT output is attenuated, its average power is measured by a power meter, while for the time-domain measurement of the baseband signal a heterodyne receiver is adopted. In particular, a passive mixer, the ZX05-43MH-S+ from MiniCircuits, is used to down-convert the signal to an IF frequency in the 100–200 MHz range, and deliver it through a low pass filter to the DSO. The DSO samples the signal at 2 GS/s, and the IQ downconversion is performed in post processing.

C. CW Measurement

The CW measurement case can be treated as a particular case of modulated signal, where an IQ modulation with constant envelope and phase is applied. The phase between BPAs and CSP inputs can be controlled by setting the phase of the IQ signals, while amplitudes can be controlled changing the carrier power.

As with the simulations, a first measurement phase has been carried out controlling manually the input power and phase relation between the BPAs and CSP inputs, in order to maintain a reasonably flat gain when the BPAs would start their compression. This permits the creation of a lookup table, that can be interpolated or fit by a function during an automatic CW power sweep.

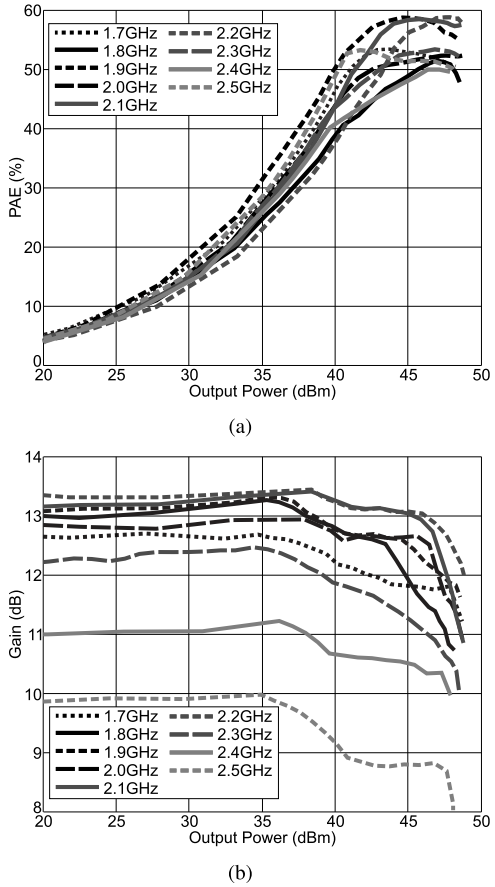

Fig. 29. Measured power sweep in the range 1.7–2.5 GHz. (a) PAE versus output power. (b) Gain versus output power.

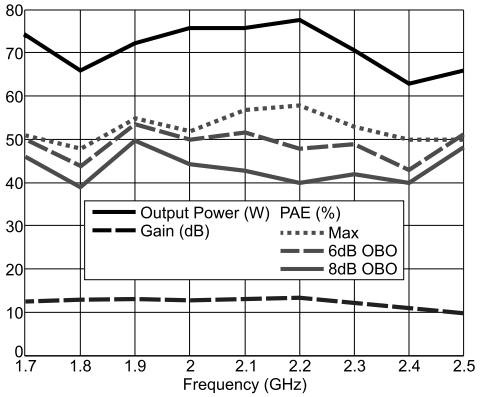

Fig. 30. CW measurements results versus center frequency.

Fig. 29 shows the measured gain (as output power divided by balanced input power) and PAE versus output power in the range 1.7–2.5 GHz. The bias is 28 V and 80 mA for the BPAs, and 28 V and gate voltage at −3.9 V for the CSP. This bias provides a rather flat gain versus drive, and it is lower than the one used for the scattering parameters measurement, as well as in simulations for the large signal analysis. As in simulations, also in this case a quadratic CSP to BPA input relation has been used, while the phase is constant versus drive, but changes frequency by frequency. Fig. 30 summarizes the main figures of merit versus CW frequency. In particular, it can

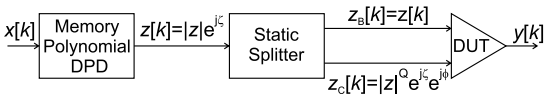

Fig. 31. Baseband equivalent block diagram of the system level characterization and linearization line-up.

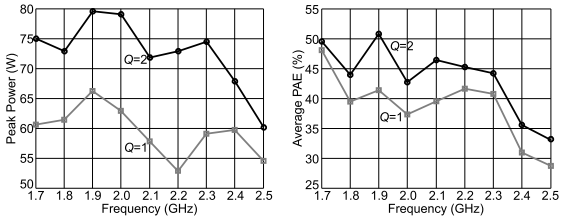

Fig. 32. Modulated measurements results. (a) Peak output power and (b) average PAE versus center frequency. Static splitter with $Q = 1$ and $Q = 2$. LTE OFDM signal with 5-MHz channel bandwidth and 9-dB PAPR.

be noticed that the maximum output power is in the range 63–78 W, with associated PAE between 48% and 58%. At 6- and 8-dB OBO, the efficiency is in the range 43%–53% and 39%–50%, respectively. Small signal gain is higher than 10 dB on the whole band. If compared to simulations, the output power is slightly lower: This could be due to thermal issues, since no cooling is applied to the devices, and modulated signal measurements can be used to confirm this cause. As expected, small signal gain is lower as well, since the BPA's bias has been reduced to maintain a flat gain versus drive response.

Table I compares the measured CW results of the proposed LMBA with other efficiency enhanced PAs with similar frequency band and output power. When considering both output power level and bandwidth, the LMBA compares well with other examples, proving that the proposed design approach can be considered as a new viable solution for active load modulated PAs.

D. Modulated Signal Results

The system level evaluation of the LMBA is based on OFDM signals for LTE downlink, with 5-MHz channel bandwidth, and PAPR of around 9 dB. The baseband equivalent of the system level setup is shown in Fig. 31. The original baseband complex signal $x[k]$ is passed through a digital predistorter (DPD), based on a memory polynomial [19] with odd nonlinear order P and memory depth M, generating the predistorted signal $z[k]$ with module $|z|$ and phase ζ. A static (without memory) splitter [20] is adopted for the generation of the balanced and CSP signals. In our case, the balanced output z_B is equal to z, while the CSP output z_C has module $|z|^Q$, with Q real, and phase $(\zeta + \phi)$, where ϕ is the configurable phase of the splitter. While the DPD function can be disabled to evaluate the intrinsic linearity of the LMBA, the static splitter is always necessary. The case with $Q = 1$ emulates a passive splitter, while a different value of Q can be used to fit the lookup table obtained from manual CW measurements. For a rather flat AM/AM response before

TABLE I
COMPARISON WITH OTHER EFFICIENCY ENHANCED BROADBAND PAS

Measurement	Unit	**This**	[5]	[9]	[10]	[11]	[12]
Frequency Range	GHz	**1.7–2.5**	1.7–2.7	1.7–2.25	1–3	1.05-2.55	1.7–2.6
$P_{\rm sat}$ Max/Min	W	**78/63**	34/16	91/66	31/20	14/10	43/29
$\rm PAE_{8dB}$ Max/Min	%	**50/39**	55/30*	50/40*	n.a.	58/35*	57/47*
$\rm PAE_{6dB}$ Max/Min	%	**53/43**	55/30*	65/53*	65/45	58/35*	57/47*
$\rm PAE_{sat}$ Max/Min	%	**58/48**	n.a.	77/65*	64/42	83/45*	66/57*
Inputs		**2**	2	1	2	1	1

* Drain Efficiency reported, PAE data not available

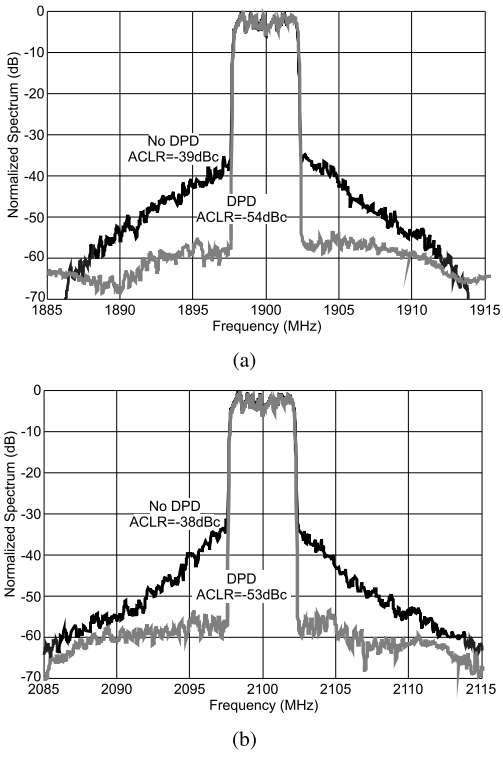

Fig. 33. Measured output spectrum of the DPA, with 5-MHz channel LTE signal and PAPR = 9 dB. Center frequency: (a) 1900 MHz and (b) 2100 MHz. Without and with DPD.

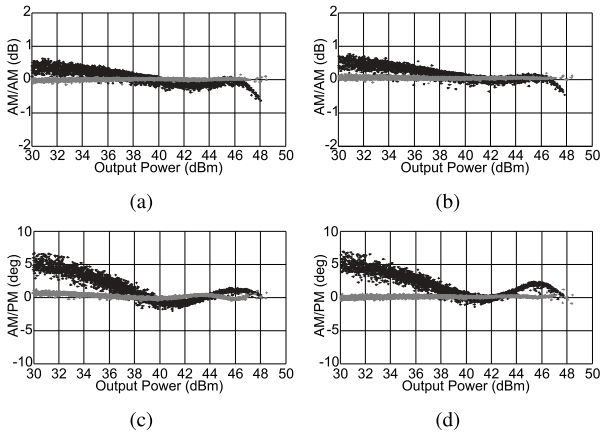

Fig. 34. (a) and (b) Measured AM/AM and (c) and (d) AM/PM with 5-MHz channel LTE signal and PAPR = 9 dB. Center frequency: (a) and (c) 1900 MHz and (b) and (d) 2100 MHz. Without (black) and with (gray) DPD.

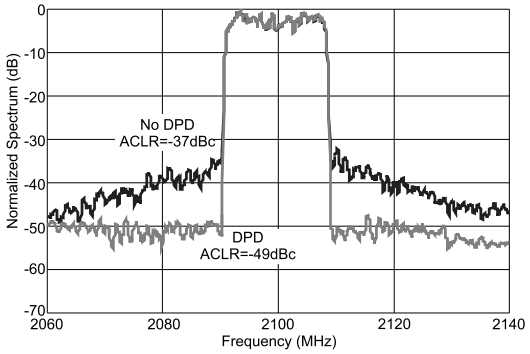

Fig. 35. Measured output spectrum of the DPA, with 20-MHz channel LTE signal and PAPR = 9 dB. Center frequency: 2100 MHz. Without and with DPD.

the break point, the BPAs are biased at 28 V and 220 mA, i.e., at higher quiescent current than in the CW case, while the CSP is still biased at 28 V, and gate at −3.9 V. Fig. 32 shows the measured peak power and average efficiency versus center frequency, comparing the cases $Q = 1$ and $Q = 2$, at constant average output power of 42 dBm (∼16 W). It can be observed how the quadratic splitter achieves higher peak power, thus reducing the AM/AM, and larger average efficiency. Fig. 33 compares the measured output spectra without and with DPD. At 1.9 GHz, the adjacent channel leakage ratio (ACLR) of −39 dBc without DPD can be reduced to −54 dBc thanks to a DPD with $P = 4$ and $M = 2$, at average power and PAE of 39.4 dBm and 46%, respectively. At 2.1 GHz, with average output power of 40 dBm and PAE of 43%, the ACLR is reduced from −38 to −53 dBc. From the same measurements, Fig. 34 shows the AM/AM and AM/PM at the two frequencies. Fig. 35 reports the measured output spectra, with and without DPD, when a 20-MHz channel LTE signal, with PAPR of 9 dB, is applied. As expected, the signal bandwidth increase leads to a worse ACLR, as well as to lower average output power and PAE, that result of 39 dBm and 40%, respectively.

V. CONCLUSION

A novel technique for efficiency enhancement in telecom PAs has been presented, based on the recently introduced LMBA. The design procedure, based on prematching networks and a dual-input architecture, has been discussed in detail, and applied to a prototype working on the 1.7–2.5-GHz band. The CW and modulated signal measurement results show the potential of the technique as a viable alternative to other efficiency enhanced PAs.

REFERENCES

[1] F. H. Raab *et al.*, "Power amplifiers and transmitters for RF and microwave," *IEEE Trans. Microw. Theory Techn.*, vol. 50, no. 3, pp. 814–826, Mar. 2002.

[2] D. J. Shepphard, J. Powell, and S. C. Cripps, "An efficient broadband reconfigurable power amplifier using active load modulation," *IEEE Microw. Wireless Compon. Lett.*, vol. 26, no. 6, pp. 443–445, Jun. 2016.

[3] A. Grebennikov and S. Bulja, "High-efficiency Doherty power amplifiers: Historical aspect and modern trends," *Proc. IEEE*, vol. 100, no. 12, pp. 3190–3219, Dec. 2012.

[4] V. Camarchia, M. Pirola, R. Quaglia, S. Jee, Y. Cho, and B. Kim, "The Doherty power amplifier: Review of recent solutions and trends," *IEEE Trans. Microw. Theory Techn.*, vol. 63, no. 2, pp. 559–571, Feb. 2015.

[5] K. Bathich, A. Z. Markos, and G. Boeck, "Frequency response analysis and bandwidth extension of the Doherty amplifier," *IEEE Trans. Microw. Theory Techn.*, vol. 59, no. 4, pp. 934–944, Apr. 2011.

[6] G. Sun and R. H. Jansen, "Broadband Doherty power amplifier via real frequency technique," *IEEE Trans. Microw. Theory Techn.*, vol. 60, no. 1, pp. 99–111, Jan. 2012.

[7] J. M. Rubio, J. Fang, V. Camarchia, R. Quaglia, M. Pirola, and G. Ghione, "3–3.6-GHz wideband GaN Doherty power amplifier exploiting output compensation stages," *IEEE Trans. Microw. Theory Techn.*, vol. 60, no. 8, pp. 2543–2548, Aug. 2012.

[8] D. Y.-T. Wu and S. Boumaiza, "A modified Doherty configuration for broadband amplification using symmetrical devices," *IEEE Trans. Microw. Theory Techn.*, vol. 60, no. 10, pp. 3201–3213, Oct. 2012.

[9] K. Bathich and G. Boeck, "Wideband harmonically-tuned GaN Doherty power amplifier," in *IEEE/MTT-S Int. Microw. Symp. Dig.*, Jun. 2012, pp. 1–3.

[10] C. M. Andersson, D. Gustafsson, J. C. Cahuana, R. Hellberg, and C. Fager, "A 1–3-GHz digitally controlled dual-RF input power-amplifier design based on a Doherty-outphasing continuum analysis," *IEEE Trans. Microw. Theory Techn.*, vol. 61, no. 10, pp. 3743–3752, Oct. 2013.

[11] R. Giofrè, L. Piazzon, P. Colantonio, and F. Giannini, "An ultra-broadband GaN Doherty amplifier with 83% of fractional bandwidth," *IEEE Microw. Wireless Compon. Lett.*, vol. 24, no. 11, pp. 775–777, Nov. 2014.

[12] J. Pang, S. He, C. Huang, Z. Dai, J. Peng, and F. You, "A post-matching doherty power amplifier employing low-order impedance inverters for broadband applications," *IEEE Trans. Microw. Theory Techn.*, vol. 63, no. 12, pp. 4061–4071, Dec. 2015.

[13] L. C. Nunes, P. M. Cabral, and J. C. Pedro, "A physical model of power amplifiers AM/AM and AM/PM distortions and their internal relationship," in *IEEE MTT-S Int. Microw. Symp. Dig.*, Jun. 2013, pp. 1–4.

[14] L. C. Nunes, P. M. Cabral, and J. C. Pedro, "AM/PM distortion in GaN Doherty power amplifiers," in *IEEE MTT-S Int. Microw. Symp. Dig.*, Jun. 2014, pp. 1–4.

[15] L. Piazzon *et al.*, "Effect of load modulation on phase distortion in Doherty power amplifiers," *IEEE Microw. Wireless Compon. Lett.*, vol. 24, no. 7, pp. 505–507, Jul. 2014.

[16] P. H. Pednekar and T. W. Barton, "RF-input load modulated balanced amplifier," in *IEEE MTT-S Int. Microw. Symp. Dig.*, Jun. 2017, pp. 1–3.

[17] R. Quaglia, M. Pirola, and C. Ramella, "Offset lines in Doherty power amplifiers: Analytical demonstration and design," *IEEE Microw. Wireless Compon. Lett.*, vol. 23, no. 2, pp. 93–95, Feb. 2013.

[18] M. Muraguchi, T. Yukitake, and Y. Naito, "Optimum design of 3-Db branch-line couplers using microstrip lines," *IEEE Trans. Microw. Theory Techn.*, vol. MTT-31, no. 8, pp. 674–678, Aug. 1983.

[19] L. Ding *et al.*, "Memory polynomial predistorter based on the indirect learning architecture," in *Proc. IEEE Global Telecommun. Conf. (GLOBECOM)*, vol. 1. Nov. 2002, pp. 967–971.

[20] J. C. Cahuana, P. Landin, D. Gustafsson, C. Fager, and T. Eriksson, "Linearization of dual-input Doherty power amplifiers," in *Proc. Int. Workshop Integr. Nonlinear Microw. Millim.-Wave Circuits (INMMiC)*, Apr. 2014, pp. 1–3.

Roberto Quaglia (M'13) was born in Casale Monferrato, Italy, in 1984. He received the Laurea degree (*cum laude*) in electronic engineering and Ph.D. degree in electronic devices from the Politecnico di Torino, Turin, Italy, in 2008 and 2012, respectively.

He is currently a Lecturer with the School of Engineering of Cardiff University, Wales, U.K. His current research interests include the design, modeling, and predistortion of high-efficiency MMIC power amplifiers.

Dr. Quaglia was a recipient of the European Union Marie Skłodowska Curie Fellow in 2015 and the 2009 Young Graduated Research Fellowship presented by the GAAS Association.

Steve Cripps (M'81–SM'90–F'11–LF'16) received the master's and Ph.D. degrees from Cambridge University, Cambridge, U.K., in 1970.

He spent many years working within the high frequency ("microwave") electronics industry in the U.K. and the USA. He was a Designer, a Manager, and an Independent Consultant. He is currently a Distinguished Research Professor with Cardiff University, Wales, U.K. He has authored several books on RF Power Amplifiers.

Dr. Cripps was a recipient of the 2008 IEEE Microwave Applications Award and the 2015 Microwave Prize. He served as an Associate Editor for IEEE MICROWAVE AND WIRELESS COMPONENTS LETTERS.